A Photoswitchable Tryptophan Zipper – (Un)folding Fibrils in Seconds

Elena Rebecca Cotroneo,[a] Tat Cheung Cheng,[b,c] Lukas Kaltschnee,[d] Patrick Maibach,[d] Moritz Engelke,[a] Niklas Schwegler,[e,f] Franziska Thomas,[f] Christina M. Thiele,[d] Nadja A. Simeth[a,c],*

[a] Institute for Organic and Biomolecular Chemistry, Department of Chemistry, University of Göttingen, Tammannstr. 2, 37077 Göttingen, Germany.
[b] Institute for Neuropathology, Department for Chemistry, University Medicine Göttingen, Robert-Koch-Strasse 40, Göttingen, Germany.
[c] Cluster of Excellence "Multiscale Bioimaging: from Molecular Machines to Networks of Excitable Cells" (MBExC), University of Göttingen, 37075 Göttingen, Germany.
[d] Clemens-Schöpf-Institute for Organic Chemistry and Biochemistry, Technical University of Darmstadt, Peter-Grünberg-Str. 16, 64287 Darmstadt, Germany.
[e] Institute for Molecular Systems Engineering and Advanced Materials (IMSEAM), Heidelberg University, Im Neuenheimer Feld 225, 69120 Heidelberg, Germany
[f] Institute of Organic Chemistry, Heidelberg University, Im Neuenheimer Feld 270, 69120 Heidelberg, Germany

Abstract

Peptides and proteins, that have the tendency to form aggregates, are often discussed in the context of Alzheimer's, Huntington's, or Parkinson's disease. However, studying aggregation processes is inherently challenging due to the due to the diversity of aggregate size and geometry and the lack of control over the aggregation process in space and time. Here, we present a small, synthetic peptide, for which aggregation can be controlled reversibly with light within seconds. Specifically, by incorporating photoswitchable unnatural amino acids into the sequence of a tryptophan zipper, we could create the A3Tz5 peptide, which can switch its secondary structure between a β-hairpin and a β-sheet-like structure through photoisomerization. We provide a detailed insight into the molecular interactions involved in this process by combining various spectroscopies and microscopy techniques. With A3Tz5 in hand, we overcame the limitation of spatiotemporal control in aggregation processes opening the door towards disease relevant studies.

Introduction

Peptide and protein aggregation is observed in many pathological conditions, such as Parkinson's, Huntington's, and Alzheimer's disease. Thus, understanding the details of aggregation mechanisms could be integral in treating and ultimately preventing these illnesses.[1,2] However, studying protein aggregation is inherently challenging due to the lack of control over it, and the complexity of the biomacromolecules.[3] To simplify the molecular structures involved, truncated versions of aggregating proteins, such as

Huntingtin,[4,5] Amyloid-ß (Aß),[6–8] or the parathyroid hormone (PTH),[9–11] are frequently used as models.

Tryptophan zippers (Tzs), on the other hand, are a family of small, synthetic peptides. They are designed to have a highly stable β-hairpin secondary structure, kept in the folded conformation by the π-π interactions of pairs of tryptophans (Trps) (Figure **1a**).[12–14] TrpZip1, a 12 amino acids peptide with the propensity to form disordered aggregates even at low concentrations, has been used as a model to understand the process of β-amyloid plaque formation.[15] Moreover, self-assembled nanofibers based on Tzs can be used to obtain biocompatible hydrogels,[16] and show antimicrobial activity supporting wound-healing.[17,18] Interestingly, the two peptides only differ in the order of two amino acids in the loop region of the hairpin: Swapping the glycine (Gly) and the asparagine (Asn) in TrpZip1 generates TrpZip2, which is better soluble and aggregates only in the matter of weeks instead of minutes.[19]

As peptides are highly sensitive to minimal structural changes, it is possible to affect their folding and thus their characteristics even through single point-mutations. By introducing stimuli-responsive amino acids, a conditional change in structure can be achieved leading to new synthetic model peptides, in which the aggregation propensity could be controlled. Light is undoubtedly the external stimulus offering the highest spatiotemporal resolution, addressing the issue of lacking temporal resolution in classical models. It has already been successfully used to remove photolabile protecting groups (PPGs) or isomerize photoswitches incorporated into peptides and proteins.[20–22] For instance, light-induced removal of a PPG on the gatekeeping Lys in $Aß_{16–22}$ and in TrpZip2 led in both cases to the disassembly of fibrils.[19,23]

More frequently, photoswitches, *i.e.* molecules that isomerize back and forth between two forms changing their characteristics, are used in peptidomimetics.[24,25] Especially, azobenzenes and stilbenes, which isomerize about a double bond between two geometrically distinct forms, were previously explored as photoswitchable turn-mimetics for β-hairpins and β-sheets.[20,22,25,26] For instance, introduction of an azobenzene moiety as backbone mimic in the Aß peptide determined its photoswitchable aggregation. Specifically, when in its *trans* isomer, the switch induced the formation of fibrils, which self-assembled in a cross-ß morphology similar to the native peptide, whereas the *cis* form showed amorphous, non-amyloid aggregates.[27] The same azobenzene was incorporated into the $(RADA)_4$ peptide backbone, and analogously shown to promote self-assembly into well-ordered fibers when in the *trans* form. In this case, the behavior could be translated into the formation of a hydrogel. Irradiation with light, accompanied by photoisomerization from the *trans* into the *cis* isomer, partially disrupted the fibers and triggered gel-sol transition.[28] Incorporation of a similar azobenzene photoswitch into $PTH_{25–37}$ in the *trans* configuration gave amyloid-like fibrils reminiscent of the parent

structure, while the *cis* form assembled into amorphous aggregates.[29] More generally, incorporation of the chromophore close to the fibril-forming region in the center of the peptide led to enhanced fibrillization in the presence of the *trans* isomer, while the aggregation was slowed down by the *cis* azobenzene.[30] A computationally optimized azobenzene backbone mimetic was introduced in a polyQ-rich amyloidogenic peptide with similar results. The peptide formed aggregates in the presence of both isomers, however, only the *cis* form could replicate the typical polyQ amyloid structure, making the compound an interesting tool for further mechanistic studies.[31] Nevertheless, the systems available so far are limited by incomplete photoisomerization or by the tendency of both photoisomers to form aggregates of different morphology.

Interestingly, light-responsive ß-hairpin mimetics have also been introduced to Tzs and could be reversibly isomerized in solution.[32] Here, the *cis* isomer serves as the turn mimetic and allows for folding of the hairpin, while the thermodynamically favorable *trans* isomer cannot adopt a fully folded hairpin structure.[32,33] When introducing a three-state molecular switch based on a stilbene motif in the loop region, the *trans* form showed sheet-like aggregates, while one of the two *cis* isomers could not be imaged by electron microscopy.[34] These studies indicate that Tzs might serve as a suitable platform to develop fully reversible, light-controllable probes for disease-relevant aggregation studies of peptides.

Reversibly light-responsive β-hairpin mimetics have, to the best of our knowledge, always been based on photoswitchable turn mimetics. However, in Tzs, the β-hairpin structure is strongly stabilized by Trp-Trp interactions (Figure **1a-b**). Therefore, we decided to attempt a destabilization of the secondary structure by substitution of the native Trp residues with photo-responsive unnatural amino acids (UAAs). This way, an altered geometry of the photoswitch upon light irradiation may generate a different steric environment in the peptide, ultimately affecting the Trp-Trp pairing and thus the correct folding of the structure. In this work, we replaced Trp residues in TrpZip2, to generate the first reported light-modulated Tz through photoswitchable amino acid side chains (Figure **1c**). We base our UAAs on heteroaryl azobenzenes as they are reported to have optimal photoswitching characteristics.[35–37] In this way, we generate reversibly light-controllable tools to investigate disease-correlated peptide aggregation with unprecedented spatiotemporal resolution.

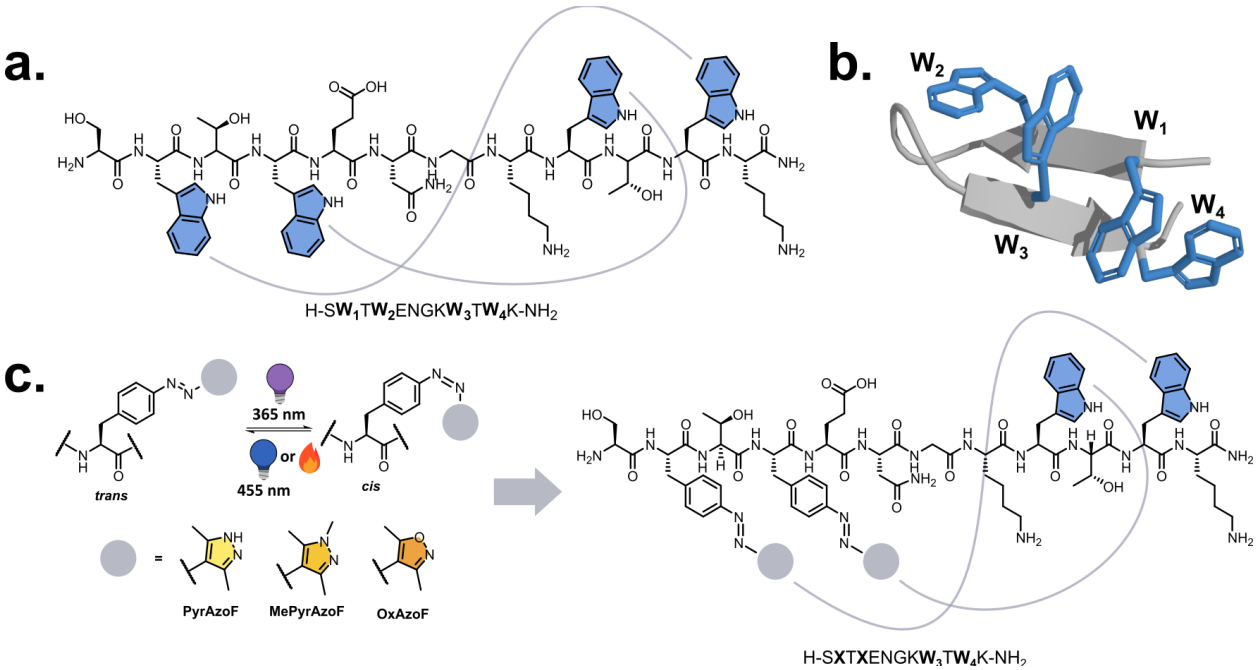

Figure 1 – **a.** Chemical structure of TrpZip2, with the tryptophan residues (W_1–W_4) highlighted in blue, and the pairing W_1-W_4 and W_2-W_3 indicated by grey lines. **b.** Pymol structure of the folded structure of TrpZip2, with the tryptophan residues (W_1-W_4) highlighted in blue (pdb 1LE1).[12] **c.** General scheme for the photoisomerization from *trans* to *cis* and back of the three UAAs (left); structure of the photoswitchable TrpZip with the incorporation of two photo-responsible UAAs in the sequence, in place of W_1 and W_2 (right) and the pairing indicated by grey lines.

Results and Discussion

In our design, we envisioned that, upon replacement of the side chains directly responsible for the stabilizing π-π interactions, the effect on the overall folding of the peptide would be highly pronounced. To realize this, we selected azo-photoswitches as lead compounds, due to their strong change in geometry from the planar *trans* into the bent *cis* isomer. Our hypothesis was that the *trans* isomer would engage in π-π interactions with the complementary Trp residue, while the *cis* form would lead to a destabilization and loss of this interaction due to a steric clash, and ultimately induce the disruption of the peptide secondary structure.

Photoswitchable Unnatural Amino Acids Synthesis and Characterization

First, we synthesized a small library of photoswitchable phenylalanine analogues to serve as light-sensitive UAAs. As mentioned before, we decided to focus our attention on heteroaromatic azo compounds, which attracted the interest of researchers only recently due their close-to-quantitative isomerization and high photoswitching quantum yields, being considered superior compared to their homoaromatic analogues.[35,38]

We started the synthesis towards the heteroaryl-compounds Fmoc-PyrAzoF-OH (**9**), Fmoc-MePyrAzoF-OH (**10**), and Fmoc-OxAzoF-OH (**11**) from the commercially available

Boc-4-amino-*L*-Phenylalanine (Figure **2a**). We began by treating the amino acid with $NaNO_2$ under acidic conditions to generate the corresponding diazonium salt. This was reacted *in situ* with 2,4-pentandione to result in the common diketone precursor **2**, adapting a reported procedure.[35,36,39] In the following step, **2** was reacted with either hydrazine, methylhydrazine, or hydroxylamine, to generate respectively the pyrazole derivative (**3**), methylated pyrazole (**4**), and isoxazole (**5**). Subsequent Boc deprotection of the *N*-terminus was conducted in DCM/TFA (1:1). Finally, to obtain SPPS-compatible building blocks, Fmoc protection with Fmoc-OSu in a mixture of $NaHCO_3$ (aq.) and MeCN (1:2) was carried out.

Whereas the synthesis of the two pyrazole-derived photoswitches proceeded with overall good yields (50% over three steps for compound **9** and 80% for compound **10**), the synthesis of the isoxazole compound (**11**) proved less efficient, with an overall yield of 6% after three steps.

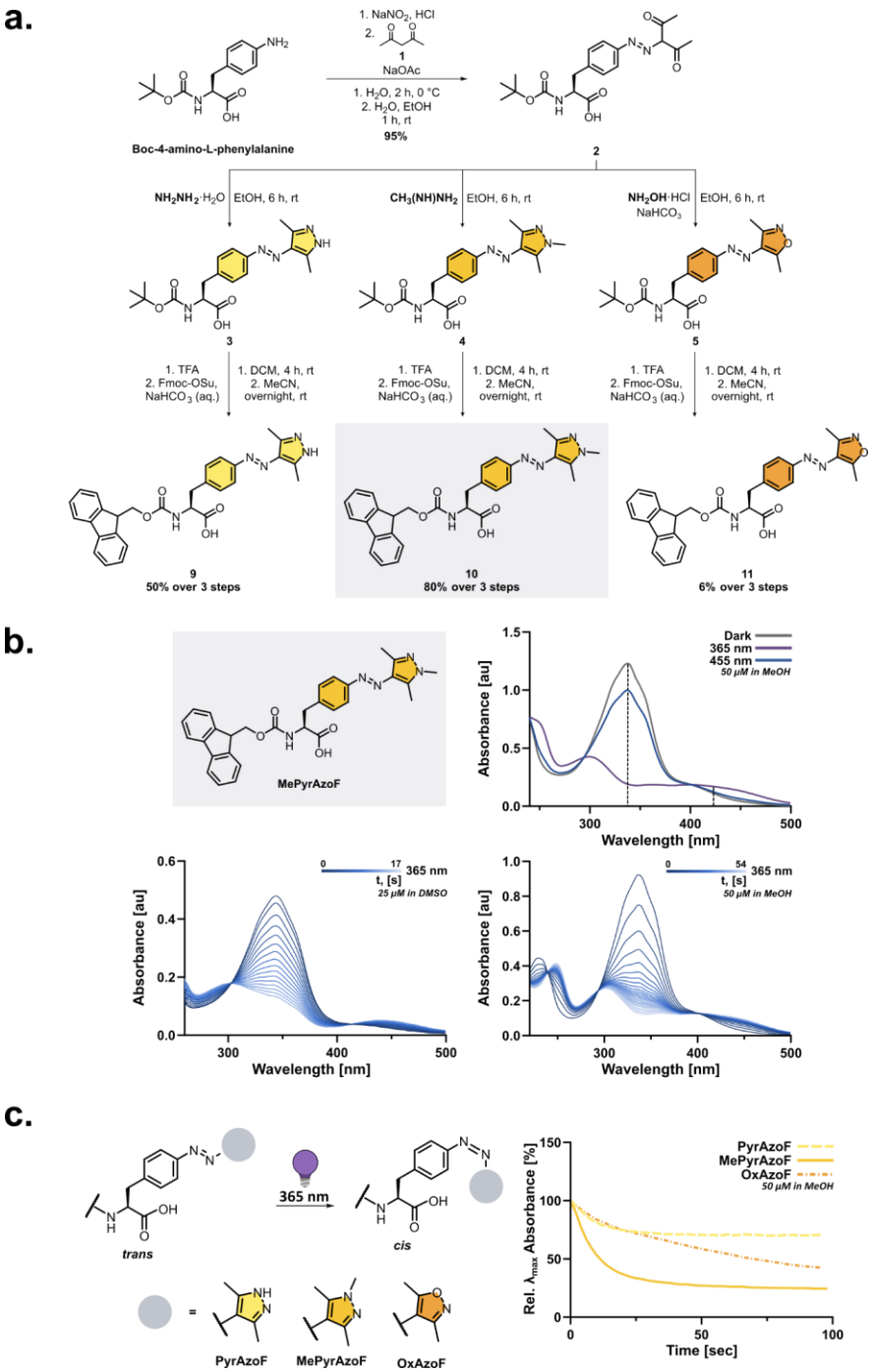

Figure 2 – **a.** Synthetic pathway to the three photoswitchable amino acids, Fmoc-PyrAzoF-OH (**9**), Fmoc-MePyrAzoF-OH (**10**), Fmoc-OxAzoF-OH (**11**). From compound **10**, the reported peptide **A3Tz5** was synthesized via microwave-assisted (MA-) SPPS. **b.** Structure of Boc-MePyrAzoF-OH, the lead photoswitchable amino acid in the series (top left); UV-Vis absorption spectrum reporting the photostationary states of the amino acid dissolved in MeOH in a 50 µM concentration (top right); photoswitching kinetics of Boc-MePyrAzoF-OH dissolved in DMSO in a 25 µM concentration (bottom left); photoswitching kinetics of Boc-MePyrAzoF-OH dissolved in MeOH in a 50 µM concentration (bottom right). All spectra were recorded at 20 °C temperature. **c.** General scheme for *trans* to *cis* photoisomerization of the three photoswitchable amino acids (left); plot reporting the percentual absorbance at the respective λ_{max} for the three *trans* isomers of the amino acids over time upon irradiation with 365 nm light (right).

Next, we investigated the photophysical and photochemical properties of both the three Boc- and the three Fmoc-protected photoswitching heteroaromatic building blocks. MeOH and DMSO were elected as solvents for the analysis to match the solubility of the molecules, since the Fmoc-protected heteroazobenzenes show scarce solubility in more protic solvents. An overview of all results is provided in Table **1** and Figure S**1**–**7**, while we will focus on discussing the characteristics recorded for Boc-protected UAAs in the next paragraphs, as more detailed analysis on them was possible due to higher solubility.

The UV-Vis absorption spectrum of Boc-PyrAzoF-OH shows the two characteristic bands of an nπ* (λ = 410 nm) and ππ* (λ = 334 nm) transition. Irradiation with 365 nm light of a sample initially kept in the dark showed the formation of the *cis* isomer, accompanied by a decrease in the band around 330 nm, while irradiation with 455 nm regenerated the original state to a large extent (Figure **S1a**). However, while recording the thermal recovery of the *trans* isomer, we found that the thermal half-life was rather short (*ca*. 3 s, MeOH at 20 °C; Figure **S2**).

Boc-MePyrAzoF-OH showed a similar band for the ππ* transition (λ = 337 nm) for the *trans* isomer, which promptly disappeared upon irradiation with 365 nm, with a quantum yield (QY) Φ = 67% in MeOH, in favor of the absorption band around 450 nm (Figure **2b, top right**), characteristic for the *cis* isomer. Analysis of the ^{1}H NMR after irradiation showed a photostationary distribution (PSD) strongly favoring the *cis* form (PSD^{365} = 4:96 [*trans*:*cis*], Table **1**, Figure **S3**). Once again, back-switching to the *trans* isomer was effective upon irradiation with 455 nm light (PSD^{455} = 79:21 [*trans*:*cis*], Table **1**, Figure **S3**). While the *trans* to *cis* isomerization proceeded almost quantitatively, blue-light illumination only resulted in the (re)generation of 79% of the *trans* isomer, which stands in contrast to literature reports.[38]

The kinetic measurements of the two pyrazole derivatives showed a similar apparent rate of light-induced *trans-cis* isomerization in DMSO (Figure **S1b** and **2b, bottom**). Changing the solvent to MeOH, the QY of the same process stayed above 50% for MePyrAzoF and the thermal half-life of its metastable *cis* isomer was largely unaffected (*ca*. 400 min). However, in the case of PyrAzoF, the thermal back isomerization in MeOH is so quick that it impairs the *trans* to *cis* light-mediated switching (*cf*. SI).

Heteroaryl-azobenzenes based on an isoxazole scaffold were introduced only recently[40] and thus, the motif was to the best of our knowledge not yet considered for the synthesis of light-responsive UAAs. The UV-Vis spectrum of Boc-OxAzoF-OH showed a hypsochromic shift in the absorption band relative to the ππ* transition (λ = 325 nm) compared to the ones of other heteroaryl-azo compounds (*vide supra*), whereas the absorption band relative to the nπ* transition remained in the same range (λ =398 nm). The same behavior as for the other UAAs upon irradiation could be observed, with a rapid decrease of the ππ* band upon exposure to 365 nm illumination with a QY of *ca*. 30% (in

MeOH, *cf*. Table **1**). The photostationary state (PSS) was observed at a 50 µM concentration in MeOD showing a PSD^{365} of 59% *trans* (Table **1**). Compared to the azopyrazole-based building blocks, the photochemical isomerization rates appeared slower under the same conditions (Figure **2b, bottom**). Irradiation with 455 nm light reverted the process, resulting in 77% *trans* (in MeOD, Table **1**) at the PSS^{455}.

Table 1 – Overview of photophysical and photochemical properties of the Boc-protected and Fmoc-protected UAAs.

Amino Acids		**Solvent**	**λ (ππ*, *trans*) [nm]**	**λ (nπ*, *trans*) [nm]**	**ε (ππ*, *trans*) [*10³ L*mol⁻¹*cm⁻¹]**	**Quantum Yield (*trans* to *cis*) [%]**	**PSD (365 nm) [trans : cis]**	**PSD (455 nm) [trans : cis]**	**λ (ππ*, cis)**	**λ (nπ*, cis)**	**$t_{1/2}$ (cis to trans) [min]**
Boc[a]	PyrAzoF	MeOH (MeOD)	334	410	22.8	n.d.[c]	n.d.[c]	n.d.[c]	229	434	3.2 s
	MePyrAzoF	MeOH (MeOD)	337	399	19.7	67	4:96	79:21	302	447	384
	OxAzoF	MeOH (MeOD)	325	398	19.3	30	42:58	79:21	307	422	930
Fmoc[b]	PyrAzoF	DMSO	344	406	n.d.	26[d]	n.d.	n.d.	313	370	n.d.
	MePyrAzoF	DMSO	344	410	n.d.	56[d]	n.d.	n.d.	310	440	424
	OxAzoF	DMSO	330	419	n.d.	17[d]	n.d.	n.d.	309	432	4537

n.d. not determined; **[a]** samples were measured at a known concentration of 50 µM; **[b]** sample concentration was calculated based on ε value of the corresponding Boc-protected UAA due to scarce solubility in DMSO; **[c]** thermal isomerization was too fast; **[d]** QY was calculated based on the ε value of the corresponding Boc-protected UAA.

Based on the photochemical and photophysical measurements, Fmoc-OxAzoF-OH was the least attractive building block for designing light-sensitive peptides, as both the speed and extent of photoswitching was less ideal compared to the pyrazole-derivatives.

By comparison of the rate of light-induced *trans* to *cis* isomerization of the three UAAs, we can see that, by irradiation with a 365 nm LED, the most favored isomerization is the one of MePyrAzoF, as it shows the highest observed photoisomerization kinetics (Figure **2c** for the Boc-protected one; full isomerization was achieved in a comparable timeframe for the Fmoc-protected MePyrAzoF in DMSO under the same irradiation conditions as per the Boc-protected precursor, see Figure S6). This can be attributed to two main reasons, namely the good overlay of the ππ* absorption band with the emission profile of the 365 nm LED, and the higher photoisomerization quantum yields of MePyrAzoF compared to the other UAAs. This important observation makes MePyrAzoF the most ideal candidate for the introduction into a peptide strand and its subsequent repeated photoswitching, as prolonged irradiation times with UV light could ultimately induce harm to the peptide.

Peptide Synthesis

After the synthesis and characterization of the three photoswitchable UAAs, we proceeded with peptide synthesis focusing on the most promising building block, MePyrAzoF. Therefore, we designed a peptide with two modifications, specifically the substitution of residues W_1 and W_2, with MePyrAzoF units (Figure **3**). This way, we aimed at disturbing the π-π interactions in both tryptophan pairs upon light irradiation, while not generating a fully synthetic photoswitch-photoswitch pair. To do so, we tested and optimized a protocol for microwave assisted solid phase peptide synthesis using an automated peptide synthesizer (details see SI).

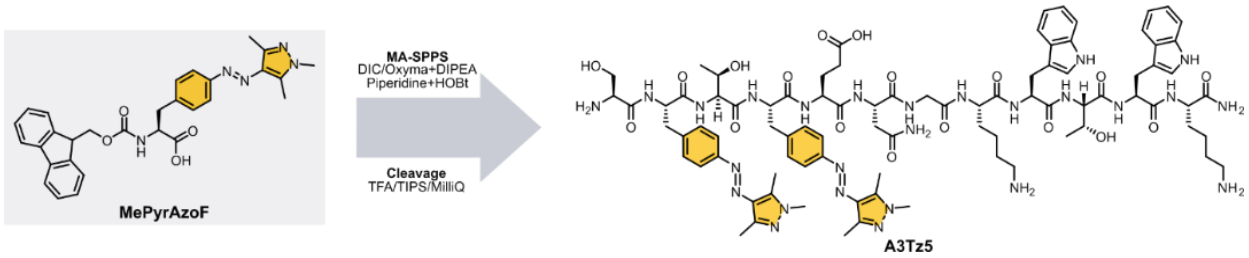

Figure 3 – Incorporation of **MePyrAzoF** in positions 2 and 4 of TrpZip2, to obtain the reported **A3Tz5** photoswitchable peptide.

For peptide coupling, the amount and concentration of Fmoc-MePyrAzoF-OH was modulated, as the non-trivial synthesis of the Fmoc-protected building block afforded only modest amounts. The optimized protocol was carried out on the synthesizer on a 25 µmol scale using a Rink Amide resin (0.37 mmol/g loading) as solid support. All natural amino acids were dissolved in DMF in a 0.2 M concentration. In the case of Fmoc-MePyrAzoF-OH, it was dissolved in a 1:5 DMSO/NMP mixture to better solubilize it, and its final concentration was reduced to 0.075 M. All amino acids were coupled twice with standard DIC/Oxyma activating conditions (with the addition of DIPEA to the Oxyma solution). The natural amino acids were used in a five-fold excess, while we reduced the equivalents of the photoswitchable building block to a three-fold excess. For deprotection, a 20% v/v

solution of piperidine in DMF was used, spiked with the addition of 0.1 M HOBt to reduce the insurgence of aspartimide formation. Standard microwave conditions as recommended by the manufacturer of the synthesizer were applied for the coupling and deprotection steps (see table **S1**).

After SPPS, the resin was collected and the peptide was cleaved from the solid support (TFA/TIPS/MilliQ, 95:2.5:2.5 v/v/v), and product formation was confirmed via ESI-MS. The crude material was purified by RP-HPLC. The final peptide, A3Tz5, was obtained after purification in a modest 12% yield, with the main side-product being identified via ESI-MS as the mono-substituted photoswitchable tryptophan zipper, likely due to the lowering of photoswitch equivalents.

Circular Dichroism Analysis

After synthesis and purification of the peptide, we performed circular dichroism (CD) spectroscopy measurements to investigate whether the substitution of Trp residues with our photoswitchable UAAs could lead to any modification in the secondary structure. To have a valid reference, we first synthesized and analyzed the native TrpZip2. The peptide has a specific CD fingerprint, with a characteristic exciton signal in the 200–250 nm region deriving from the π-π interactions between its two tryptophan pairs (Figure **4a**), making it straightforward to confirm whether the secondary structure would be affected by our modification or not.[12]

Upon dissolution of A3Tz5 in PBS buffer, we observed a singular behavior. A3Tz5 generated large, yellow aggregates visible to the naked eye (Figure **S7a**). We decided to record a CD spectrum of the initial sample kept in the dark, which showed a peculiar fingerprint (Figure **4b**). A positive band, which we associated with the nπ* transition of the trans isomer of the photoswitch, was visible between 400 and 500 nm. Furthermore, in the region between 300 and 190 nm, which is usually characterized by defined bands used to identify peptide secondary structures, new unknown signals were observed. In particular, the only one that could be reconducted to a known secondary structure motif was the one between 190 and 250 nm, with a clear minimum at 218 nm, indicating that the peptide has a pronounced β-sheet content. Furthermore, the intensity of the signal was very low, which we attributed to the fact that most of the peptide was not in solution. Notably, β-hairpins are reported to aggregate into β-amyloid-like structures.[41] We assumed that this could be the same for A3Tz5, as this would explain both the CD signature and the macroscopic aggregates observed in the cuvette.

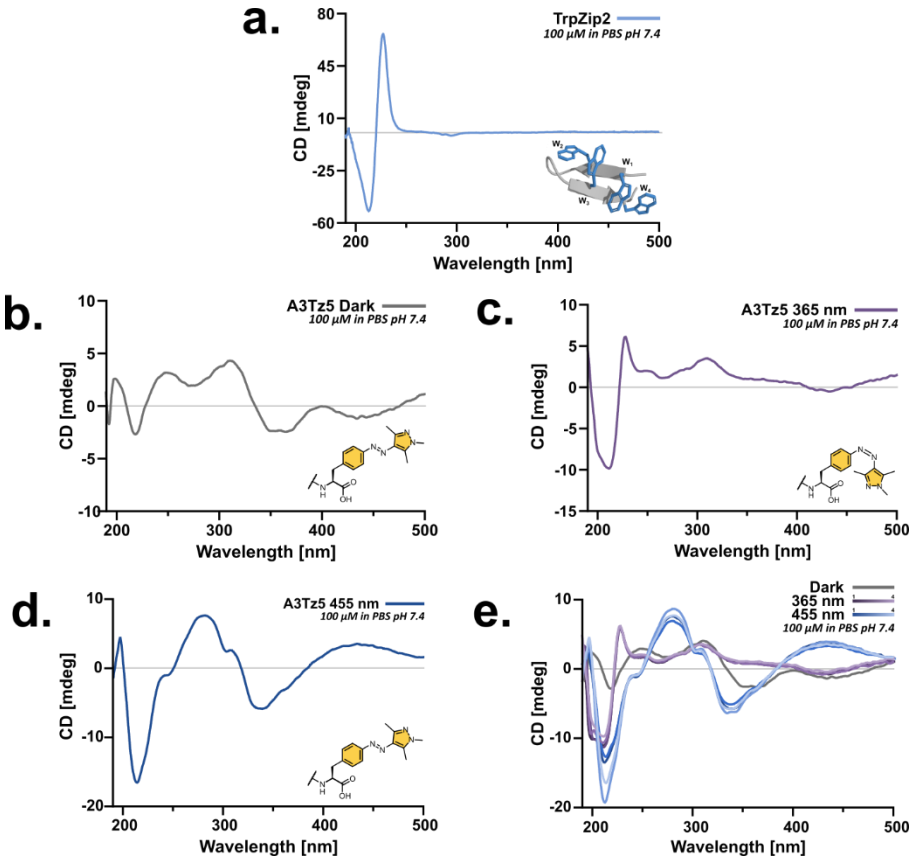

Figure 4 – **CD Spectroscopy** – **a.** CD spectrum of native tryptophan zipper TrpZip 2 recorded at 20 °C, dissolved in PBS buffer (pH 7.4, 10 mM) in a 100 µM concentration. The characteristic exciton signal with a maximum at 227 nm and a minimum at 212 nm indicates a folded β-hairpin structure. **b.** CD spectrum of a 100 µM sample of A3Tz5 dissolved in PBS (10 mM) kept in the dark, with the two UAAs in *trans* configuration; **c.** CD spectrum of the A3Tz5 sample after 15 min of irradiation at 365 nm, with the two UAAs in *cis* configurations; **d.** CD spectrum of the A3Tz5 sample after 15 min of irradiation at 455 nm with the two UAAs in *trans* configuration; **e.** Overlapped CD spectra of the A3Tz5 sample (*previa* irradiation, irradiated at 365 nm, irradiated at 455 nm, repeated cycles). All spectra were recorded at 20 °C.

We decided to irradiate the sample with 365 nm light to investigate whether we could still photoswitch the MePyrAzoF residues in the peptide and in this way disrupt the aggregates. After 15 minutes of illumination with a 365 nm LED, we observed the complete dissolution of the yellow aggregates and the simultaneous yellowing of the solution (Figure **S7b**). We promptly recorded a CD spectrum of the sample, and this time we could identify the characteristic fingerprint of a β-hairpin structure (Figure **4c**). This finding would indicate that the *cis* isomer of the photoswitch is able to interact with its complementary Trp residue in the zipper structure, which goes against our original hypothesis. Furthermore, a band at around 300–330 nm emerged. A similar band has been previously reported in literature and has been attributed to a modification in the angle of interaction between a 3-methyl-indole Trp residue and an unmodified pairing Trp.[42] The positive band in the 300 nm region would be derived from an increased overlapping of the five membered rings of the indoles. In our case, we could assume that the methyl-pyrazoles in position 2 and 4 are at a similar angle when in their *cis* form,

broadly overlapping with the five membered rings of W_3 and W_4. This change in geometry and its respective CD band emerging would support the hypothesis that the photoswitchable UAA is able to collaboratively interact with its Trp partner.

We then irradiated the sample once more, this time with 455 nm wavelength light, to see whether we would reform the macrostructures of the original sample. After 15 minutes of blue light irradiation, we could clearly observe the fading of the yellow hue in the solution, accompanied by the formation of fibril-like colorless macrostructures, once again clearly visible to the naked eye (Figure **S7c**). After performing CD analysis on the sample, we were presented with yet a new spectrum, with a maximum at 280 nm, and an intense minimum at 212 nm (Figure **4d**). This new fingerprint, to the best of our knowledge, does not correspond to any reported peptide secondary structure. To verify whether this was indeed a stable structure, we performed cycles of light irradiation at 365 and 455 nm and recorded a CD spectrum each time. As shown in Figure **4e**, the two secondary structures attributed to *trans*-A3Tz5 (at PSS^{455}) and *cis*-A3Tz5 (at PSS^{365}) were stable over multiple repetitions.

Ultimately, what we could gain from a qualitative analysis of the CD spectra was that A3Tz5 presents at least three different secondary structures which give origin to different states. While the trans isomer of the photoswitchable UAAs is always associated with the formation of macrostructures, the cis isomer seems to promote the correct folding of the peptide into a β-hairpin-like structure, thus inducing dissolution into the buffer.

NMR Analysis

To get a more detailed insight into the structural features of the photo-peptide and its self-assembly properties, we performed solution state NMR studies, using a modified setup for in-situ sample illumination[43–45] to follow the photo-switching process (see sections 1.4. and 5. of the SI). The presence of large aggregates (>20 kDa) in solution or peptides being in the solid state in the *trans* configuration prior to irradiation became immediately evident by the lack of signal in solution state ^{1}H-NMR (Fig. **5a**, black spectrum). Subsequent in-situ irradiation with a 370 nm LED, which should promote *trans* to *cis* isomerization of the UAA residues, solubilized the photo-peptide and defined signals could be identified (Figure **5a**, purple spectra). Importantly, the process was reversible by irradiation with 455 nm light, and disappearance of signal from the ^{1}H-NMR spectrum was observed, likely due to the formation of larger aggregates and possible precipitation (Figure **5a**, blue spectra). We repeated the photoswitching between solution and solid states several times (Figure **5a** and **b**) and, like in CD-spectroscopy (*vide supra*), obtained the same spectra after each cycle, indicating a high reproducibility of the same 3D structures of A3Tz5.
Both, in this and in other analytical techniques (*cf*. CD-spectroscopy above or microscopy below), promoting the initial sample into the dissolved state proceeded slower than from

the solid-state generated through irradiation with 455 nm (see rate constants in Table S6). We presume that this is due to a structure of comparably higher order being formed upon slow aggregation, compared to the morphology of the aggregates formed upon 455 nm irradiation (*cf*. CD spectra above and microscopy below).

Notably, when we exposed the sample of A3Tz5 in the dark to prolonged irradiation with 370 nm light to solubilize a maximum amount of material, we did not succeed to convert the full amount of A3Tz5 peptide into liquid-state NMR observable species. In all cases the peptide concentration estimated from the ^{1}H-NMR integrals was significantly lower than the nominal peptide concentration estimated from the weighed peptide mass (see concentrations in Table S4). The maximum liquid-state NMR detectable fraction of the peptide remained between 13% and 23% of the full amount of peptide in the sample, so the majority of the compound remained in larger aggregates (>20 kDa) or in the solid.

In addition to this, the NMR data collected features clear indications for self-aggregation of A3Tz5, including the dependence of chemical shifts, line-widths, and relaxation parameters on the peptide concentration (Figure **5d-e** and Figure S11 and Tables S5 & S6). The most striking change is observed in the ^{1}H relaxation time constants (T_1 and T_2) of the samples with 1 mM and 5 mM A3Tz5 concentration: Between 1 mM and 5 mM, the peptide seems to transition from the "fast/intermediate tumbling limit", to the "slow tumbling limit",[46,47] as apparent from T_1 times (see Tables S5 & S6). At 1 mM concentration, T_1 times vary across the different chemical shift ranges, which is indicative of rotational diffusion in solution faster than the Larmor-frequency ($\tau_c < (2\pi\ 700\ \mathrm{MHz})^{-1}$ in this case, with τ_c being the rotational correlation time), whereas a five-fold increase in concentration suffices to obtain practically uniform T_1 times across the full peptide, which is indicative for rotational diffusion much slower than the Larmor-frequency ($\tau_c \gg (2\pi\ 700\ \mathrm{MHz})^{-1}$). This points at a strong increase of the aggregate size in the single-digit mM concentration range.

As a consequence of aggregation, relaxation parameters are unfavorable for collection of signal assignment spectra. Amongst the 2D correlation spectra collected (see Figures S13 – S16), only NOESY spectra provided correlations into the backbone. In all other cases only sidechain correlations were observed. This points at a notable rigidification of the backbone during self-aggregation. Due to the spectral quality obtained, only TOCSY and NOESY spectra provided useful information for ^{1}H-signal assignment. Despite this limitation, it was possible to assign a large fraction of the ^{1}H-residues with confidence (66% – 85%, see Table S7). During assignment, only a single set of ^{1}H-signals was found for A3Tz5. This indicates that amongst the four configurational isomers expected due to switching of the photoswitchable groups,[48] only one isomer forms species that are sufficiently small to be detectable by solution-state NMR. The other three configurational isomers seem to precipitate or to form large aggregates.

To interrogate the fold obtained, we collected NOESY experiments with sufficient signal-to-noise to identify inter-residue NOE contacts. Indeed, in particular in the methyl region

of the sidechains, inter-residue NOE contacts can be identified, indicating spatial proximity between the photoswitchable sidechains (residues 2 & 4 MePyrAzoF) and the tryptophan sidechains (residues 9 & 11 Trp). Specifically, all three methyl groups in the 1,2,4-trimethylpyrazole-moieties of both MePyrAzoF residues show clear NOE contacts to 11 Trp Hδ and to 11 Trp $H_{\zeta 1}$. In addition to the contacts between the aromatic residues, NOE cross-peaks are also clearly observed between 3 Thr ($CH_{3,\gamma}$) and 11 Trp Hδ as well as between 3 Thr ($CH_{3,\gamma}$) and a ^{1}H at 7.09 ppm (9 Trp Hδ, 9 Trp $H_{\eta 1}$ or 11 Trp $H_{\zeta 2}$, Figure **5e** and **f**), clearly supporting a fold with close contact of the respective aromatic residues. Together with our earlier observation of an excitation signal in CD-spectroscopy, which indicated the presence of a β-hairpin structure, the results from the NMR experiments strongly corroborate a folded conformation of the photo-peptide when the UAA residues are in the *cis* forms, likely due to π-π-interactions of the aromatic residues.

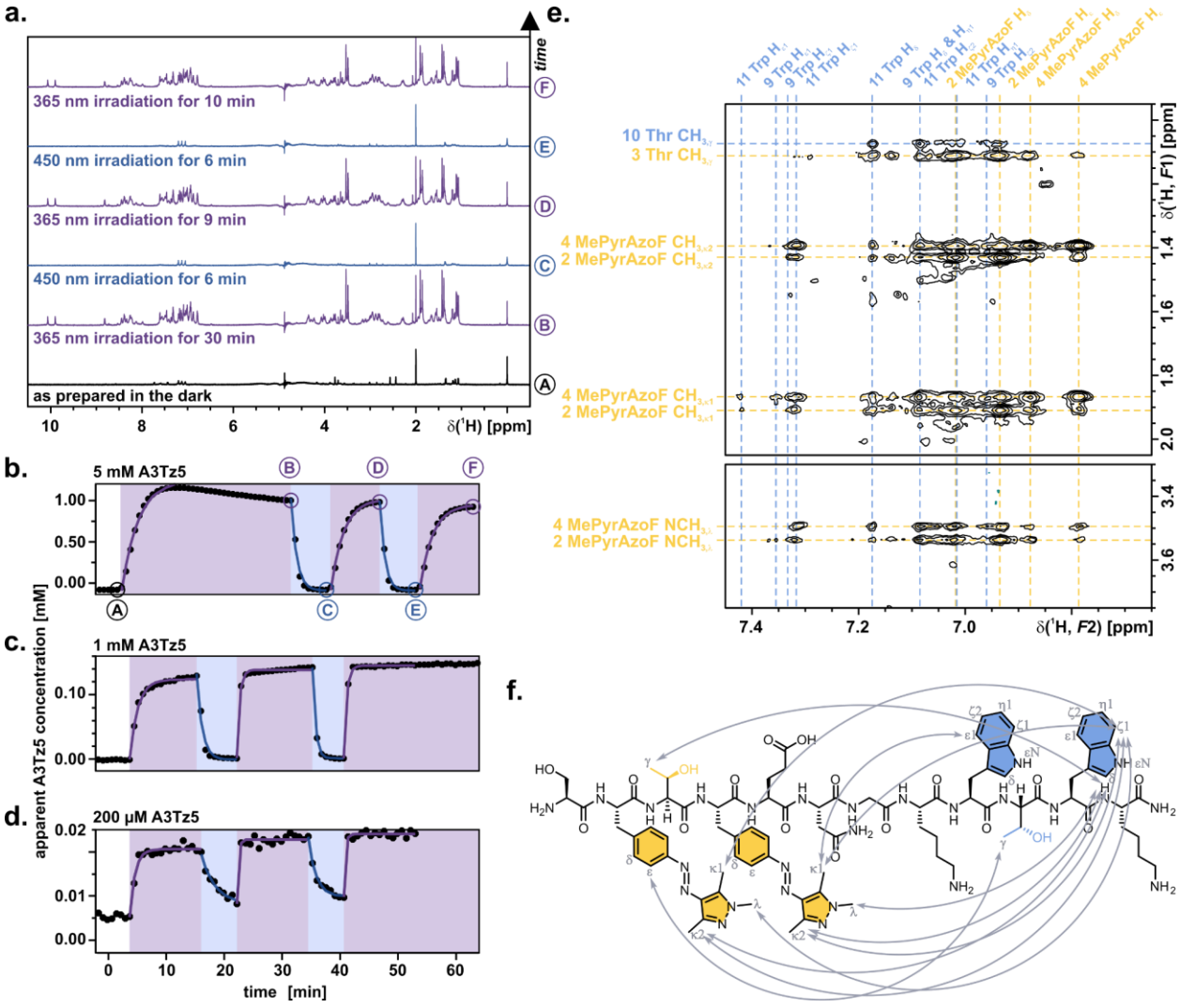

Figure 5 – **NMR Spectroscopy** – **a.** ^{1}H-NMR spectra of A3Tz5 obtained with in-situ illumination in the NMR. The spectra shown were taken at time points A – F, marked in Panel b., in a series of spectra collected with alternating sample irradiation with 370 nm or 455 nm light. Spectra were collected with the

sample with a nominal 5 mM A3Tz5 concentration, using water suppression.[49] **b. – d.** Apparent A3Tz5 concentration estimated from the ^{1}H spectrum integrals measured in series of water-suppressed ^{1}H-spectra measured with in-situ illumination. Periods of irradiation with 370 nm or 455 nm light are highlighted in magenta or blue, respectively. A transparent background signifies no irradiation. Monoexponential fits to the measured integrals are shown as purple or blue lines, and fitting values are summarized in Table S4. To reduce the integral offset originating from a non-zero baseline due to water suppression, the averaged spectra before irradiation were subtracted from all spectra prior to integration. Panels b., c. and d. were collected for samples with nominal A3Tz5 concentrations of 5 mM, 1 mM and 200 µM, respectively. **e.** Excerpt of a NOESY experiment showing the methyl-to-aromatics correlation region for A3Tz5. The full spectrum is shown in Figure S13b. Data was collected with continuous irradiation at 370 nm, using the sample with a nominal 5 mM A3Tz5 concentration and a 200 ms mixing time. To facilitate the identification of inter- -residue NOE contacts which may indicate spatial proximity between the A3Tz5 and the Trp residues, residues 2 – 4 are marked in yellow, whereas labels residues 9 – 11 are marked in blue. **f.** Mapping of selected intra-residue NOE contacts between residues 2 – 4 and residues 9 – 11. All NMR data shown was collected at 15 °C, and all NMR samples were prepared in PBS buffer (pH 7.4, 10 mM, 8% ^{2}H) containing 0.094 mM TSP-d_4.

Light and Electron Microscopy

Following the CD measurements, and the observation of stable macrostructures visible with the naked eye, we decided to attempt further visual investigation through different microscopy techniques. We began by recording the photoswitching of an A3Tz5 sample (200 µM in PBS buffer at pH 7.4) by use of a digital light microscope. We zoomed into the sample to a final magnification of 200x, and we proceeded to irradiate the sample first with 365 nm light for about 30 minutes, after which we could observe complete dissolution of the large, yellow aggregates. We then alternatively irradiated with a 455 nm LED and a 365 nm LED light for a total of *ca*. 40 repetitions, with an average irradiation time of 10 seconds with UV light, and 20 seconds with blue light. We video recorded the process (see Supporting Information) showing that the formation and dissolution of the fibrillar macroaggregates is reproducible over numerous irradiation cycles, and fully reversible in the timespan of 30 seconds (Figure 6a).

To better understand the nanostructure of the aggregates, we proceeded to image A3Tz5 via Cryo scanning electron microscope (SEM) and Cryo transmission electron microscopy (TEM). All samples were prepared by dissolving an aliquot of peptide into PBS buffer at pH 7.4 to a final concentration of 50 µM. CryoSEM imaging was performed on all three states of the sample (dark, 365 nm, 455 nm), but did not prove reproducible in the case of the 455 nm irradiated one. What we could observe in the dark sample (Figure **6b, top**) was the presence of large, apparently disordered aggregates with dimensions averaging around 50 µm. CryoSEM imaging of a second sample, irradiated with 365 nm, shows disappearance of such aggregates (Figure **6b, bottom**), supporting the information gained with CD and NMR spectroscopy which suggests a higher grade of dissolution of the peptide. Multiple attempts were carried out to provide CryoSEM imaging of a third sample, irradiated with 455 nm light, but results have not been reproducible.

To gain information regarding the nanostructure of the different states we further investigated the samples by CryoTEM imaging. In this case, the grid loaded with the dark

sample showed no presence of nanostructures (Figure **S8**). We attributed this to the fact that the majority of the peptide is involved in the formation of the macroaggregates imaged via CryoSEM, which are too big to be observed by CryoTEM. In the case of the sample irradiated with 365 nm light, we once again were presented with an empty grid (Figure **6c, top**) which we could attribute this time to the fact that most of the peptide is in solution, thus too small to be observed by CryoTEM imaging. Last, we imaged the sample irradiated with 455 nm light, and in this case, we could observe the formation of long, regular, and ordered double stranded fibrils (Figure **6c, bottom**). Further investigation of the samples through 2D averaging over 2000 images confirmed the presence of fibrillar structures, which presented as either single filaments or double stranded filaments (Figure **6d**).

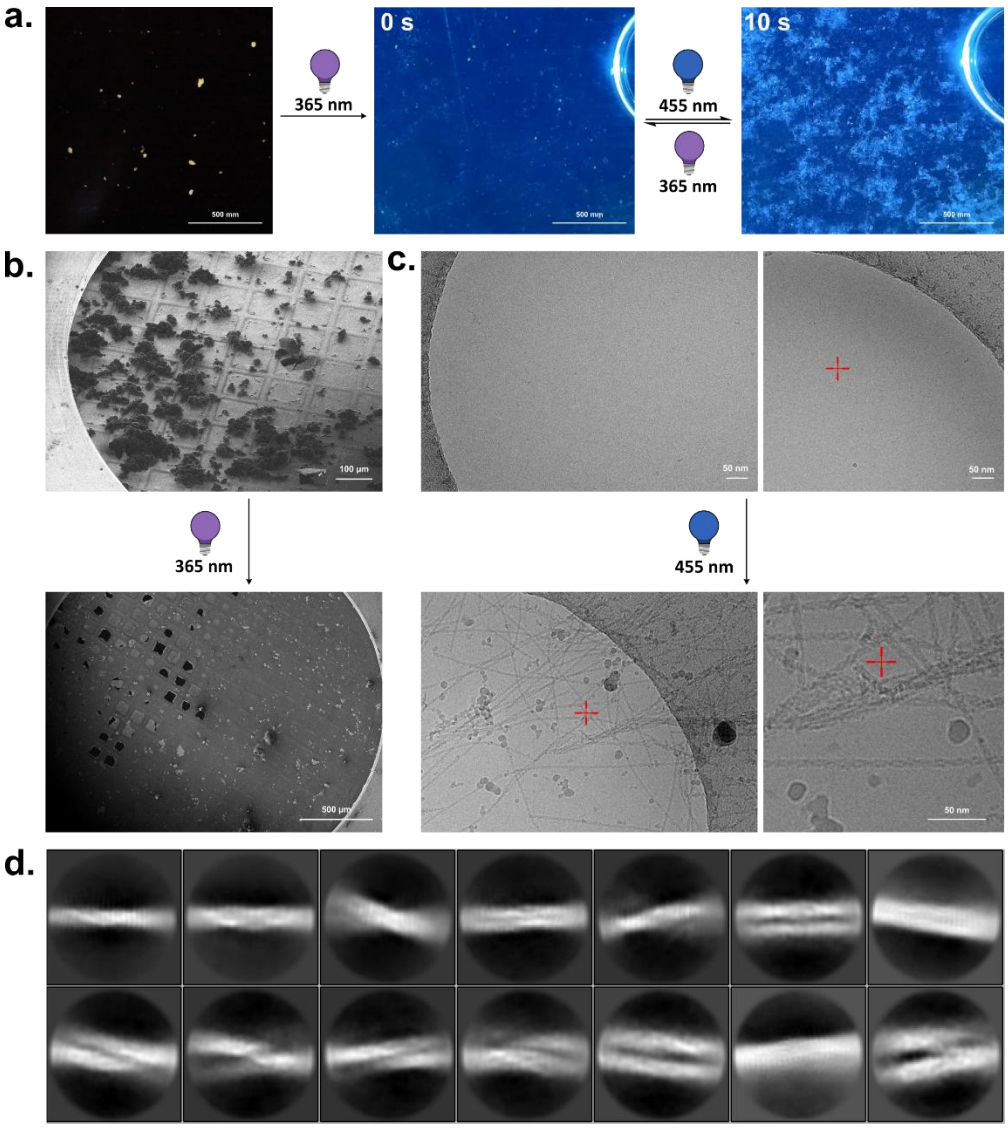

Figure 6 – **Microscopy** – **a.** Light microscope recording of the photoswitching ability of A3Tz5 and consequent self-assembly. From the yellow aggregates of the sample *previa* irradiation (left), to a clear solution after irradiation with 365 nm light (middle), to the reversible formation of stable aggregates upon

irradiation with 455 nm light (right). **b.** CryoSEM imaging of an A3Tz5 sample kept in the dark (magnification 200x, top) and CryoSEM imaging of an A3Tz5 sample after irradiation with 365 nm light (magnification 69x, bottom); **c.** CryoTEM imaging of an A3Tz5 sample after irradiation with 365 nm light (magnification 64kx, top); CryoTEM imaging of an A3Tz5 sample after irradiation with 455 nm light (magnification 64kx and 165kx, bottom); **d.** CryoTEM 2D averaging of the A3Tz5 sample irradiated with 455 nm light.

Ultimately, CryoSEM and CryoTEM imaging allowed us to understand the (nano)structure of our photoswitchable aggregates. In particular, we could confirm that the geometry and shape of the aggregates in the dark state and after irradiation with 455 nm look significantly different, with the latter looking extremely ordinate and fibrillar at least in the nanoscale, and that irradiation with UV light (365 nm) seems to dissolve the peptide, leading to oligomeric hairpin structures in solution.

Conclusions

In conclusion, we presented, to the best of our knowledge, the first ever reported tryptophan zipper with light-controlled UAA-tryptophan pairs. With this new system we were able to effectively photoswitch in real time the secondary structure of the peptide between one soluble and folded β-hairpin, and one aggregating β-sheet-like form.

From the three photoswitchable UAAs synthesized and studied, we selected Fmoc-MePyrAzoF-OH as the light-responsive core with the most desirable properties, including high QY and PSD, and sufficient thermal stability of the metastable form, for the final construct. The microwave-assisted, automated SPPS of the A3Tz5 peptide was successfully carried out, and two photoswitchable UAAs featuring a phenylazopyrazole motif were incorporated into a Tz to generate the corresponding UAA-tryptophan hetero pairs. We characterized the structure of A3Tz5 in the dark and the photochemically generated states from the molecular to the microscopic scale, to obtain a full picture of its light-controllable behavior combining UV-Vis, CD, and in-situ irradiation NMR spectroscopy, and different imaging techniques. We observed that upon dissolution in PBS buffer, the peptide aggregates into disordered macrostructures of *ca*. 50 µm (CryoSEM) visible to the naked eye, with a β-sheet character observed via CD spectroscopy. NMR analysis proved that in this state, the vast majority of the peptide is, indeed, in the solid state. A possible explanation for this structure is the abrupt exposure to the solvent, which does not allow time for an ordered structure to be formed.

Upon irradiation with UV light, we could observe an almost complete dissolution of the aggregates, and in this state, CD also shows a tendency of A3Tz5 towards folding into a β-hairpin, suggesting that the positive interactions between the photoswitches and the corresponding Trp residues are achieved while the UAAs are in their *cis* configuration. This finding is supported both by the presence of the characteristic exciton signal in the CD spectrum and by the 2D NMR studies showing interactions between the methyl groups of the photoswitch with the indole ring of the tryptophan moiety. Both CD and NMR

analysis suggest that the folded peptide assembles into a soluble, oligomeric form resulting in structures too small to be imaged by CryoSEM or CryoTEM.

Furthermore, irradiation with 455 nm light and accompanied *cis* to *trans* isomerization led to the formation of a new macrostructure with a strikingly distinct CD fingerprint compared to initial aggregates formed in the dark. CryoTEM confirmed the presence of large fibrils that have a defined and ordered nanostructure with twisted single or double filaments. We hypothesize that the comparably slow increase in concentration of the unfolded peptide with UAAs in *trans* configuration allowed for a controlled supramolecular self-assembly of the peptide into the fibers, potentially supported by intermolecular interactions between the *trans* UAAs. Importantly, the nanofilaments are formed and unformed over numerous cycles of light irradiation, and the general structure does not seem to be altered by repeated switches.

To our best knowledge, this is the first system that switch between a discrete β-hairpin structure and fibrillar β-sheet nanostructures by point mutation of tryptophan residues and thus modulation of the π-π interactions between amino acid residues in the sequence. Our approach allowed us to achieve unprecedented fast response times generating and dissolving fibrillar nanostructures with a recorded time of 30 seconds to achieve a full cycle. We can envision that this novel system could be applied for the investigation of pathological peptide aggregation leading to a deeper understanding of its mechanism and eventually open the door for the development of new therapies.

Acknowledgements

ERC thanks the Hertha Sponer College. We thank Pia Weigel, Ole Specht, Maximilian Winkler, and Dr. Nico Graw for their fantastic technical support. N.S. is grateful to the Evangelisches Studienwerk Villigst e.V. for support through a Doctoral Scholarship and to the Joachim Herz Foundation for support through the Add-On Fellowship for Interdisciplinary Life Sciences. LK and CMT thank the DFG for funding through the CRC 1194 (project No 265191195). This work was funded by the Deutsche Forschungsgemeinschaft (DFG, German Research Foundation) under Germany's Excellence Strategy (EXC 2067/1-390729940 to NAS). This research project was financially supported by the state of Lower-Saxony and the VolkswagenFoundation, Hannover, Germany. Cryo-ET instrumentation was jointly funded by the DFG Major Research Instrumentation program (448415290) and the Ministry of Science and Culture of the State of Lower Saxony.

References

(1) Irvine, G. B.; El-Agnaf, O. M.; Shankar, G. M.; Walsh, D. M. Protein Aggregation in the Brain: The Molecular Basis for Alzheimer's and Parkinson's Diseases. *Mol. Med.* **2008**, *14* (7–8), 451–464. https://doi.org/10.2119/2007-00100.Irvine.

(2) Salahuddin, P.; Fatima, M. T.; Uversky, V. N.; Khan, R. H.; Islam, Z.; Furkan, M. The Role of Amyloids in Alzheimer's and Parkinson's Diseases. *Int. J. Biol. Macromol.* **2021**, *190*, 44–55. https://doi.org/10.1016/j.ijbiomac.2021.08.197.
(3) Housmans, J. A. J.; Wu, G.; Schymkowitz, J.; Rousseau, F. A Guide to Studying Protein Aggregation. *FEBS J.* **2023**, *290* (3), 554–583. https://doi.org/10.1111/febs.16312.
(4) Arribat, Y.; Bonneaud, N.; Talmat-Amar, Y.; Layalle, S.; Parmentier, M.-L.; Maschat, F. A Huntingtin Peptide Inhibits PolyQ-Huntingtin Associated Defects. *PLoS ONE* **2013**, *8* (7), e68775. https://doi.org/10.1371/journal.pone.0068775.
(5) Arndt, J. R.; Chaibva, M.; Legleiter, J. The Emerging Role of the First 17 Amino Acids of Huntingtin in Huntington's Disease. *Biomol. Concepts* **2015**, *6* (1), 33–46. https://doi.org/10.1515/bmc-2015-0001.
(6) Hawk, L. M. L.; Pittman, J. M.; Moore, P. C.; Srivastava, A. K.; Zerweck, J.; Williams, J. T. B.; Hawk, A. J.; Sachleben, J. R.; Meredith, S. C. B-amyloid Model Core Peptides: Effects of Hydrophobes and Disulfides. *Protein Sci.* **2020**, *29* (2), 527–541. https://doi.org/10.1002/pro.3778.
(7) Frieg, B.; Han, M.; Giller, K.; Dienemann, C.; Riedel, D.; Becker, S.; Andreas, L. B.; Griesinger, C.; Schröder, G. F. Cryo-EM Structures of Lipidic Fibrils of Amyloid-β (1-40). *Nat. Commun.* **2024**, *15* (1), 1297. https://doi.org/10.1038/s41467-023-43822-x.
(8) Valiente-Gabioud, A. A.; Riedel, D.; Outeiro, T. F.; Menacho-Márquez, M. A.; Griesinger, C.; Fernández, C. O. Binding Modes of Phthalocyanines to Amyloid β Peptide and Their Effects on Amyloid Fibril Formation. *Biophys. J.* **2018**, *114* (5), 1036–1045. https://doi.org/10.1016/j.bpj.2018.01.003.
(9) Chen, L.; Xiong, L.; Yao, L.; Pan, J.; Arzola, E.; Zhu, X.; Mei, L.; Xiong, W.-C. Attenuation of Alzheimer's Brain Pathology in 5XFAD Mice by PTH1-34, a Peptide of Parathyroid Hormone. *Alzheimers Res. Ther.* **2023**, *15* (1), 53. https://doi.org/10.1186/s13195-023-01202-z.
(10) Dettori, C.; Ronca, F.; Scalese, M.; Saponaro, F. Parathyroid Hormone (PTH)-Related Peptides Family: An Intriguing Role in the Central Nervous System. *J. Pers. Med.* **2023**, *13* (5), 714. https://doi.org/10.3390/jpm13050714.
(11) Rendina-Ruedy, E.; Rosen, C. J. Parathyroid Hormone (PTH) Regulation of Metabolic Homeostasis: An Old Dog Teaches Us New Tricks. *Mol. Metab.* **2022**, *60*, 101480. https://doi.org/10.1016/j.molmet.2022.101480.
(12) Cochran, A. G.; Skelton, N. J.; Starovasnik, M. A. Tryptophan Zippers: Stable, Monomeric β-Hairpins. *Proc. Natl. Acad. Sci.* **2001**, *98* (10), 5578–5583. https://doi.org/10.1073/pnas.091100898.
(13) Wu, L.; McElheny, D.; Huang, R.; Keiderling, T. A. Role of Tryptophan−Tryptophan Interactions in Trpzip β-Hairpin Formation, Structure, and Stability. *Biochemistry* **2009**, *48* (43), 10362–10371. https://doi.org/10.1021/bi901249d.
(14) Pham, T. L.; Thomas, F. Design of Functional Globular β-Sheet Miniproteins. *ChemBioChem* **2024**, *25* (7), e202300745. https://doi.org/10.1002/cbic.202300745.
(15) Bruździak, P.; Panuszko, A.; Piotrowski, B.; Stangret, J. Structural Changes of a Simple Peptide—Trpzip-1—in Aqueous Solutions and the Corresponding Hydration Phenomena under the Influence of Temperature. *J. Mol. Liq.* **2019**, *277*, 532–540. https://doi.org/10.1016/j.molliq.2018.12.101.
(16) Nguyen, A. K.; Molley, T. G.; Kardia, E.; Ganda, S.; Chakraborty, S.; Wong, S. L.; Ruan, J.; Yee, B. E.; Mata, J.; Vijayan, A.; Kumar, N.; Tilley, R. D.; Waters, S. A.; Kilian, K. A. Hierarchical Assembly of Tryptophan Zipper Peptides into Stress-Relaxing Bioactive Hydrogels. *Nat. Commun.* **2023**, *14* (1), 6604. https://doi.org/10.1038/s41467-023-41907-1.
(17) Xu, L.; Chou, S.; Wang, J.; Shao, C.; Li, W.; Zhu, X.; Shan, A. Antimicrobial Activity and Membrane-Active Mechanism of Tryptophan Zipper-like β-Hairpin Antimicrobial Peptides. *Amino Acids* **2015**, *47* (11), 2385–2397. https://doi.org/10.1007/s00726-015-2029-7.
(18) Li, B.; Ouyang, X.; Liu, Y.; Ba, Z.; Yang, Y.; Zhang, J.; Yang, P.; Yang, T.; Wang, Y.; Zhao, Y.; Mao, W.; Zhong, C.; Liu, H.; Zhang, Y.; Gou, S.; Ni, J. Novel β-Hairpin Antimicrobial Peptide Containing the β-Turn Sequence of -NG- and the Tryptophan Zippers Facilitate Self-Assembly into Nanofibers, Exhibiting Excellent Antimicrobial Performance. *J. Med. Chem.* **2024**, *67* (8), 6365–6383. https://doi.org/10.1021/acs.jmedchem.3c02339.
(19) Markiewicz, B. N.; Oyola, R.; Du, D.; Gai, F. Aggregation Gatekeeper and Controlled Assembly of Trpzip β-Hairpins. *Biochemistry* **2014**, *53* (7), 1146–1154. https://doi.org/10.1021/bi401568a.
(20) Peddie, V.; Abell, A. D. Photocontrol of Peptide Secondary Structure through Non-Azobenzene Photoswitches. *J. Photochem. Photobiol. C Photochem. Rev.* **2019**, *40*, 1–20. https://doi.org/10.1016/j.jphotochemrev.2019.05.001.

(21) Brieke, C.; Rohrbach, F.; Gottschalk, A.; Mayer, G.; Heckel, A. Light-Controlled Tools. *Angew. Chem. Int. Ed.* **2012**, *51* (34), 8446–8476. https://doi.org/10.1002/anie.201202134.
(22) Albert, L.; Vázquez, O. Photoswitchable Peptides for Spatiotemporal Control of Biological Functions. *Chem. Commun.* **2019**, *55* (69), 10192–10213. https://doi.org/10.1039/C9CC03346G.
(23) Measey, T. J.; Gai, F. Light-Triggered Disassembly of Amyloid Fibrils. *Langmuir* **2012**, *28* (34), 12588–12592. https://doi.org/10.1021/la302626d.
(24) Robinson, J. A. β-Hairpin Peptidomimetics: Design, Structures and Biological Activities. *Acc. Chem. Res.* **2008**, *41* (10), 1278–1288. https://doi.org/10.1021/ar700259k.
(25) Erdélyi, M.; Varedian, M.; Sköld, C.; Niklasson, I. B.; Nurbo, J.; Persson, Å.; Bergquist, J.; Gogoll, A. Chemistry and Folding of Photomodulable Peptides – Stilbene and Thioaurone-Type Candidates for Conformational Switches. *Org. Biomol. Chem.* **2008**, *6* (23), 4356. https://doi.org/10.1039/b812001c.
(26) Podewin, T.; Rampp, M. S.; Turkanovic, I.; Karaghiosoff, K. L.; Zinth, W.; Hoffmann-Röder, A. Photocontrolled Chignolin-Derived β-Hairpin Peptidomimetics. *Chem. Commun.* **2015**, *51* (19), 4001–4004. https://doi.org/10.1039/C4CC10304A.
(27) Doran, T. M.; Anderson, E. A.; Latchney, S. E.; Opanashuk, L. A.; Nilsson, B. L. An Azobenzene Photoswitch Sheds Light on Turn Nucleation in Amyloid-β Self-Assembly. *ACS Chem. Neurosci.* **2012**, *3* (3), 211–220. https://doi.org/10.1021/cn2001188.
(28) Doran, T. M.; Ryan, D. M.; Nilsson, B. L. Reversible Photocontrol of Self-Assembled Peptide Hydrogel Viscoelasticity. *Polym. Chem.* **2014**, *5* (1), 241–248. https://doi.org/10.1039/C3PY00903C.
(29) Paschold, A.; Voigt, B.; Hause, G.; Kohlmann, T.; Rothemund, S.; Binder, W. H. Modulating the Fibrillization of Parathyroid-Hormone (PTH) Peptides: Azo-Switches as Reversible and Catalytic Entities. *Biomedicines* **2022**, *10* (7), 1512. https://doi.org/10.3390/biomedicines10071512.
(30) Paschold, A.; Schäffler, M.; Miao, X.; Gardon, L.; Krüger, S.; Heise, H.; Röhr, M. I. S.; Ott, M.; Strodel, B.; Binder, W. H. Photocontrolled Reversible Amyloid Fibril Formation of Parathyroid Hormone-Derived Peptides. *Bioconjug. Chem.* **2024**, *35* (7), 981–995. https://doi.org/10.1021/acs.bioconjchem.4c00188.
(31) Parlato, R.; Volarić, J.; Lasorsa, A.; Bagherpoor Helabad, M.; Kobauri, P.; Jain, G.; Miettinen, M. S.; Feringa, B. L.; Szymanski, W.; Van Der Wel, P. C. A. Photocontrol of the β-Hairpin Polypeptide Structure through an Optimized Azobenzene-Based Amino Acid Analogue. *J. Am. Chem. Soc.* **2024**, *146* (3), 2062–2071. https://doi.org/10.1021/jacs.3c11155.
(32) Dong, S.; Löweneck, M.; Schrader, T. E.; Schreier, W. J.; Zinth, W.; Moroder, L.; Renner, C. A Photocontrolled β-Hairpin Peptide. *Chem. – Eur. J.* **2006**, *12* (4), 1114–1120. https://doi.org/10.1002/chem.200500986.
(33) Spekowius, J.; Pfister, R.; Helbing, J. Folding and Unfolding of the Tryptophan Zipper in the Presence of Two Thioamide Substitutions. *J. Phys. Chem. B* **2021**, *125* (28), 7662–7670. https://doi.org/10.1021/acs.jpcb.1c03327.
(34) Poloni, C.; Stuart, M. C. A.; Van Der Meulen, P.; Szymanski, W.; Feringa, B. L. Light and Heat Control over Secondary Structure and Amyloid-like Fiber Formation in an Overcrowded-Alkene-Modified Trp Zipper. *Chem. Sci.* **2015**, *6* (12), 7311–7318. https://doi.org/10.1039/C5SC02735G.
(35) Calbo, J.; Weston, C. E.; White, A. J. P.; Rzepa, H. S.; Contreras-García, J.; Fuchter, M. J. Tuning Azoheteroarene Photoswitch Performance through Heteroaryl Design. *J. Am. Chem. Soc.* **2017**, *139* (3), 1261–1274. https://doi.org/10.1021/jacs.6b11626.
(36) Stricker, L.; Fritz, E.-C.; Peterlechner, M.; Doltsinis, N. L.; Ravoo, B. J. Arylazopyrazoles as Light-Responsive Molecular Switches in Cyclodextrin-Based Supramolecular Systems. *J. Am. Chem. Soc.* **2016**, *138* (13), 4547–4554. https://doi.org/10.1021/jacs.6b00484.
(37) Stricker, L.; Böckmann, M.; Kirse, T. M.; Doltsinis, N. L.; Ravoo, B. J. Arylazopyrazole Photoswitches in Aqueous Solution: Substituent Effects, Photophysical Properties, and Host–Guest Chemistry. *Chem. – Eur. J.* **2018**, *24* (34), 8639–8647. https://doi.org/10.1002/chem.201800587.
(38) Weston, C. E.; Richardson, R. D.; Haycock, P. R.; White, A. J. P.; Fuchter, M. J. Arylazopyrazoles: Azoheteroarene Photoswitches Offering Quantitative Isomerization and Long Thermal Half-Lives. *J. Am. Chem. Soc.* **2014**, *136* (34), 11878–11881. https://doi.org/10.1021/ja505444d.
(39) Torii, K.; Hori, Y.; Watabe, K.; Kikuchi, K. Development of Photoswitchable Fluorescent Molecules Using Arylazopyrazole. *Bull. Chem. Soc. Jpn.* **2020**, *93* (7), 821–824. https://doi.org/10.1246/bcsj.20200077.

(40) Kumar, P.; Srivastava, A.; Sah, C.; Devi, S.; Venkataramani, S. Arylazo-3,5-dimethylisoxazoles: Azoheteroarene Photoswitches Exhibiting High *Z* -Isomer Stability, Solid-State Photochromism, and Reversible Light-Induced Phase Transition. *Chem. – Eur. J.* **2019**, *25* (51), 11924–11932. https://doi.org/10.1002/chem.201902150.
(41) Larini, L.; Shea, J.-E. Role of β-Hairpin Formation in Aggregation: The Self-Assembly of the Amyloid-β(25–35) Peptide. *Biophys. J.* **2012**, *103* (3), 576–586. https://doi.org/10.1016/j.bpj.2012.06.027.
(42) Roy, A.; Bouř, P.; Keiderling, T. A. TD-DFT Modeling of the Circular Dichroism for a Tryptophan Zipper Peptide with Coupled Aromatic Residues. *Chirality* **2009**, *21* (1E). https://doi.org/10.1002/chir.20792.
(43) Feldmeier, C.; Bartling, H.; Riedle, E.; Gschwind, R. M. LED Based NMR Illumination Device for Mechanistic Studies on Photochemical Reactions – Versatile and Simple, yet Surprisingly Powerful. *J. Magn. Reson.* **2013**, *232*, 39–44. https://doi.org/10.1016/j.jmr.2013.04.011.
(44) Nitschke, P.; Lokesh, N.; Gschwind, R. M. Combination of Illumination and High Resolution NMR Spectroscopy: Key Features and Practical Aspects, Photochemical Applications, and New Concepts. *Prog. Nucl. Magn. Reson. Spectrosc.* **2019**, *114–115*, 86–134. https://doi.org/10.1016/j.pnmrs.2019.06.001.
(45) Ji, Y.; DiRocco, D. A.; Kind, J.; Thiele, C. M.; Gschwind, R. M.; Reibarkh, M. LED-Illuminated NMR Spectroscopy: A Practical Tool for Mechanistic Studies of Photochemical Reactions. *ChemPhotoChem* **2019**, *3* (10), 984–992. https://doi.org/10.1002/cptc.201900109.
(46) Bloembergen, N.; Purcell, E. M.; Pound, R. V. Relaxation Effects in Nuclear Magnetic Resonance Absorption. *Phys. Rev.* **1948**, *73* (7), 679–712. https://doi.org/10.1103/PhysRev.73.679.
(47) Kowalewski, J.; Maler, L. *Nuclear Spin Relaxation in Liquids: Theory, Experiments, and Applications*, 0 ed.; CRC Press, 2006. https://doi.org/10.1201/9781420012194.
(48) Kind, J.; Kaltschnee, L.; Leyendecker, M.; Thiele, C. M. Distinction of Trans–Cis Photoisomers with Comparable Optical Properties in Multiple-State Photochromic Systems – Examining a Molecule with Three Azobenzenes via in Situ Irradiation NMR Spectroscopy. *Chem. Commun.* **2016**, *52* (84), 12506–12509. https://doi.org/10.1039/C6CC06771A.
(49) Hwang, T. L.; Shaka, A. J. Water Suppression That Works. Excitation Sculpting Using Arbitrary Wave-Forms and Pulsed-Field Gradients. *J. Magn. Reson. A* **1995**, *112* (2), 275–279. https://doi.org/10.1006/jmra.1995.1047.